Original Research Paper

Analysis of particle rotation in fluidized bed by use of discrete particle model

Run-Jia Liu [a,b], Rui Xiao [a,*], Mao Ye [b,*], Zhongmin Liu [b]

[a] *Key Laboratory of Energy Thermal Conversion and Control of Ministry of Education, College of Energy and Environmental Engineering, Southeast University, Nanjing 210096, China*
[b] *National Engineering Laboratory for MTO, Dalian Institute of Chemical Physics, Chinese Academy of Sciences, Dalian 116023, China*

ABSTRACT

The particle rotation was found important in the fluidized bed when the heterogeneous structures appeared. Some researches show that Magnus lift force might play an pivotal role in fluid-solid system, especially when the particles have fast rotation speed. As the Magnus lift force is acted at the single particle level, a pseudo two-dimensional discrete particle model (DPM) was used to investigate the influence of Magnus lift force in fluidized bed. The rotational Reynolds number (Re_r) bases on the angular velocity and the diameter of the spheres is used to characterize the rotational movement of particles. We studied the influence of Magnus lift force for particles with rotational Reynolds number in the range of 1–100. Our results show that the influence of Magnus lift force is enhanced with a higher Re_r. Magnus lift force affects the movement of particles in both radial and axial directions while Re_r is high. However, in low Re_r case it can be neglected in computational simulation model. This indicates the introduction of Magnus lift force may improve the discrete particle model only in high Re_r case and Magnus effect should be considered in real gas-solid two phase system when the particle rotational speed is high.

© 2018 The Society of Powder Technology Japan. Published by Elsevier B.V. and The Society of Powder Technology Japan. All rights reserved.

1. Introduction

Recent years have seen a rapid growth of interests in detailed particles motion in a wide variety of natural and industrial processes. Particle motion possesses significant influence on the hydrodynamics in these processes. For example, in industrial fluidized beds such as circulating fluidized bed (CFB) risers, the particles experience not only translational but also rotational motion due to the frequent particle-particle collisions and the relative velocity between solids and the surrounding airflow [1]. Particle rotation appears to have effect on the linearity of the motion and may play a part in the mechanism of particle entrainment in conveyed solid-gas system [2].

Some experimental methods was used to track particle rotation and analyzed relevant influence factors such as particle size, average particle collision velocity, particle collision rate and particle number density [3]. Other researchers tried to obtain the angular velocity by use of the digital imaging method. For example, with a high-speed digital camera system, Wu et al. [3,4] measured the averaged particles rotational velocity in a cold CFB riser. They found the mean rotational velocity for particles with a density of

2400–2600 kg/m^3 and size of 0.5 mm was about 300 rev/s whilst the highest rotational velocity could be up to 2000 rev/s. The study on particle rotation, however, still presents a big challenge since the direct measurement of particle angular velocity is, if not impossible, extremely hard.

Relatively more contributions have been made to numerical study of particle in solid-gas two-phase flows [5]. In the interesting work by Kajishima et al. [6], they found that, due to the reverse direction of lift force in the shear flows, the irrotational particles could be easily absorbed into clusters but rotational ones might escape. Similar conclusion can be found by Wang et al. [7] who argue that particle rotation reduce the cluster size. Sun et al. [8] found that the multi-fluid model taking the particle rotation into account could better capture the bubble dynamics and time-averaged bed behavior in fluidized bed. Despite the significance of particle rotation in solid-gas two-phase flows found in the aforementioned studies, much are yet to be understood on how the particle rotation affects hydrodynamics.

It is widely accepted that the rotational particles experience a Magnus lift force, which is perpendicular to the plane constituted by particle translational and rotating velocities. The Magnus lift force was first discovered by Newton in 1671 [9], and the Magnus effect in particle systems has since been a subject to many investigations [10–13]. Oliver [10] attempted to explain some

* Corresponding authors.
E-mail addresses: ruixiao@seu.edu.cn (R. Xiao), maoye@dicp.ac.cn (M. Ye).

Nomenclature

C_d	drag coefficient, [–]	U	fluid velocity, m/s
d_p	particle diameter, mm	u_x	fluid velocity at X-direction, m/s
$F_{ab,n}$	normal contact force, N	u_y	fluid velocity at Y-direction, m/s
$F_{ab,t}$	tangential contact force, N	u_z	fluid velocity at Z-direction, m/s
$F_{cont,a}$	contact force, N	v_a	particle normal velocity, m/s
$F_{dra,a}$	drag force, N	v_{ab}	relative velocity, m/s
F_L	lift force, N	V	volume of fluid cell, m^3
$F_{mag,a}$	magnus lift force, N	V_a	volume of particle, m^3
g	gravity acceleration, m/s^2		
p	pressure, Pa	*Greek symbols*	
Re	Reynolds number, [–]	ε	porosity, [–]
Re_r	rotational Reynolds number, [–]	η	damping coefficient, N s/m
k	spring stiffness, N/m	ρ_g	gas density, kg/s^3
m_a	particle mass, kg	δ_n	overlap, m
n_{ab}	normal unit vector, [–]	δ_t	tangential displacement, m
N_{part}	number of particles, [–]	$\bar{\tau}$	viscous stress tensor, kg/m s^2
n	number of fluctuant particles, [–]	Θ_a	angular displacement, [–]
I_a	moment of inertia, kg m^2	μ_f	friction coefficient, [–]
S_p	source term symbol, kg/(m^2/s^2)	μ_g	dynamic viscosity, Pa s
t	time, s	ω	rotational speed, 1/s
T_a	particle torque, N m		

phenomena and behavior of particle in tubes by using Magnus effect. White and Schulz [13] studied the motion of spherical glass microbeads (of diameter 350 um and density 2.5 g/cm^3) in a wind tunnel, and found that their results could be well explained by the Magnus effect. Lukerchenko [12] found the existence of Magnus effect in solid particle saltation over rough bed in a numerical study, and Huang et al. [11] further demonstrated the trajectories of saltating grains could be influenced by the Magnus effects. Dandy and Dwyer [14] compared the Magnus lift force and drag force acting on a particle over a wide range of Reynolds number, and showed the magnitude of the Magnus lift force was far less than that of drag force. You et al. [15] also think that for a small size particle, even if the speed reaches 10^6 rev/min, the lift force can be neglected as compared with the drag force. However, in a very recent work Zhou and Fan [16] studied the solid-fluid interaction by use of an immersed boundary lattice Boltzmann simulations, and their results suggest that the Magnus force might become even larger than the drag force in case of high Reynolds number and low solid volume fraction in particulate flows.

A natural question thus is whether the influence of particle rotation, especially the Magnus lift force, can be ignored or not in fluidized bed reactors. In this work, we aim at the study of Magnus lift force on the hydrodynamics of fluidized beds by use of discrete particle model. The underlying inspiration is that the discrete particle model can be used as an efficient learning tool for solid-gas interaction at particle level. According to Zhou and Fan [16], the Magnus effect is more pronounced for high Re and low solid volume fractions. Therefore in this research we will focus on the particle rotation and Magnus effect in circulating fluidized bed (CFB) risers. Our results show that the influence of Magnus lift force is enhanced with a higher Re_r. Magnus lift force affects the movement of particles in both radial and axial directions while Re_r is high. However, in low Re_r case it can be neglected in computational simulation model. This indicates the introduction of Magnus lift force may improve the discrete particle model only in high Re_r case and Magnus effect should be considered in real gas-solid two phase system when the particle rotational speed is high.

2. Mathematical model

The DPM-code was originally developed by Kuipers et al. and has been validated and extensively applied in various solid-gas two-phase systems [17–19].

2.1. Gas phase

The gas flow is described by the volume-averaged Navier-Stokes equation [20]:

$$\frac{\partial(\varepsilon\rho_g)}{\partial t} + (\nabla \cdot \varepsilon\rho_g u) = 0 \tag{1}$$

$$\frac{\partial(\varepsilon\rho_g u)}{\partial t} + (\nabla \cdot \varepsilon\rho_g uu) = -\varepsilon\nabla p - S_p - \nabla \cdot (\varepsilon\bar{\tau}) + \varepsilon\rho_g g \tag{2}$$

where ε presents the porosity, g the gravity acceleration, ρ_g the gas density, u the gas velocity, $\bar{\tau}$ the viscous stress tensor, and p the pressure of the gas phase. Based on the Newton's third law, the equivalent of that force must be acting on the mesh cell that the particle resides in. So the Magnus effect on gas phase should have been considered in Eq. (2). The solution in our study is to correct source term S_p. The source term S_p is:

$$S_p = \frac{1}{V} \int \sum_{a=0}^{N_{part}} [F_{dra,a} + F_{mag,a}]\delta(r - r_a)dV \tag{3}$$

where V is the volume of fluid cell, V_a the volume of particle, v_a the particle velocity, and N_{part} the number of particles. The δ-function is to ensure the reaction force acts as a point force at the position of the particle [21]. $F_{dra,a}$ and $F_{mag,a}$ are drag force and Magnus lift force which will be discussed in Section 2.2.3. To solve the pressure linked equation, the SIMPLE algorithm is used in this research [22].

2.2. Particle phase

In the DPM model, the Newton's second law is used to track the velocity and position of each particle:

$$m_a \frac{d^2 r_a}{dt^2} = F_{cont,a} + F_{mag,a} + F_{dra,a} - V_a \nabla p + m_a g \qquad (4)$$

$$I_a \frac{d^2 \Theta_a}{dt^2} = T_a \qquad (5)$$

where m_a is the mass of particle, I_a the moment of inertia, Θ_a the angular displacement, and T_a the torque of particle. In this research we consider three types of force acting on the particles: the contact force $F_{cont,a}$, the drag force $F_{dra,a}$ and the Magnus lift force $F_{mag,a}$.

2.2.1. Contact force

The contact force $F_{cont,a}$ includes both normal and tangential component,

$$F_{cont,a} = \sum_{contactlist} (F_{ab,n} + F_{ab,t}) \qquad (6)$$

In this research the linear-spring/dashpot soft-sphere model [23] is used to calculate the contact force. The normal and tangential component are respectively given by:

$$F_{ab,n} = -k_n \delta_n n_{ab} - \eta_n v_{ab,n} \qquad (7)$$

and

$$F_{ab,t} = \begin{cases} -k_t \delta_t - \eta_t v_{ab,t}, & for \ |F_{ab,t}| \leqslant \mu_f |F_{ab,n}| \\ -\mu_f |F_{ab,n}| t_{ab}, & for \ |F_{ab,t}| > \mu_f |F_{ab,n}| \end{cases} \qquad (8)$$

Here k is the spring stiffness, η the damping coefficient, n_{ab} the normal unit vector, δ_n the overlap, δ_t the tangential displacement, μ_f the friction coefficient and v_{ab} the relative velocity between two particles. More information about this model can be found in [24].

2.2.2. Drag force

The traditional drag model, which is a combination of Ergun equation for dense regime and Wen-Yu correlation for dilute regime, is used in this research [25,26]:

$$F_{dra,a} = 3\pi \mu_g \varepsilon^2 d_p (\vec{u} - \vec{v}_a) f(\varepsilon) \qquad (9)$$

$$f(\varepsilon) = \begin{cases} \frac{150(1-\varepsilon)}{18\varepsilon^3} + \frac{1.75}{18} \frac{Re_p}{\varepsilon^3}, & \varepsilon < 0.8 \\ \frac{C_d}{24} Re_p \varepsilon^{-4.65}, & \varepsilon \geqslant 0.8 \end{cases} \qquad (10)$$

Here the particle Reynolds number $Re_p = \frac{\varepsilon d_p (\vec{u} - \vec{v}) \rho_g}{\mu_g}$, where ε is the void fraction, d_p the diameter of particle, and μ_g the dynamic viscosity. The drag coefficient $C_d = \frac{24}{Re_p} (1 + \frac{3}{16} Re_p)$ follows Oseen [27].

2.2.3. Magnus lift force

The calculation of the Magnus lift force follows Zhou & Fan [16]:

$$F_L = \frac{3\pi \mu_g d_p \vec{u} Re_r}{\varepsilon^2} [-0.0398(1-\varepsilon) + 0.0317] \qquad (11)$$

Here the rotational Reynolds number $Re_r = \frac{\rho_g \vec{\omega} d_p^2}{\mu_g}$, where ω is the particle rotational velocity, and u the velocity of fluid. In their study, Zhou and Fan introduced a coordinate frame with the origin fixed at the center of particle, and thus the translational motion of particle can be ignored in the calculations. In this research, we used a coordinate frame with the origin fixed at the wall of reactor, and thus the Magnus force is calculated as:

$$F_{mag,a} = \frac{3\pi[-0.0398(1-\varepsilon) + 0.0317]\rho_g d_p^3}{\varepsilon^2} \vec{\omega} \times (\vec{v}_a - \vec{u})$$
$$= \frac{3\pi[-0.0398(1-\varepsilon) + 0.0317]\rho_g d_p^3}{\varepsilon^2} \begin{vmatrix} i & j & k \\ \omega_x & \omega_y & \omega_z \\ v_{x,a} - u_x & v_{y,a} - u_y & v_{z,a} - u_z \end{vmatrix} \qquad (12)$$

And the three components of the Magnus force are:

$$\begin{cases} F_{xmag,a} = \frac{3\pi[-0.0398(1-\varepsilon) + 0.0317]\rho_g d_p^3}{\varepsilon^2} [\omega_y (v_{z,a} - u_z) - \omega_z (v_{y,a} - u_y)] \\ F_{ymag,a} = \frac{3\pi[-0.0398(1-\varepsilon) + 0.0317]\rho_g d_p^3}{\varepsilon^2} [\omega_z (v_{x,a} - u_x) - \omega_x (v_{z,a} - u_z)] \\ F_{zmag,a} = \frac{3\pi[-0.0398(1-\varepsilon) + 0.0317]\rho_g d_p^3}{\varepsilon^2} [\omega_x (v_{y,a} - u_y) - \omega_y (v_{x,a} - u_x)] \end{cases} \qquad (13)$$

2.3. Numerical simulations

The schematic diagram of the pseudo-2D gas-fluidized bed is shown in Fig. 1. The depth of the bed is the diameter of a single particle. In total $25 \times 1 \times 300$ fluid grid cells are used in this research. The simulation parameters are listed in Table 1. Most parameters follows the experiments and simulations by Mathiesen et al. [28]. A mixture of two kinds of particles is considered. The time step is estimated by the method of Tsuji et al. [29]:

$$\Delta t < \frac{2}{5} \pi \sqrt{\frac{m_a}{k}} \qquad (14)$$

Before the formal simulation experiment, particle-wall contact should be discussed, which occurs frequently in a reactor or channel [30–32]. And particle-wall contact may cause erosion on the pipe. Salaei et al. [33] discussed particle erosion in a 90°pipe bend. They found particle erosion happened on the bend area. In this study, a cuboid model was built to simulate fluidized bed. Therefore, No-slip boundary is used for the four sidewalls [18], the fluid phase influx cell (gas inlet boundary) is set at the bottom of the bed where the gas is injected, and the prescribed cell (pressure outlet boundary) is set at the top of the bed. Particles are settled in the bottom of the bed at the beginning. When a particle reaches the top boundary a new one will be introduced to enter the bottom, so the number of particles in bed will be a constant. The turbulence is not consider in this study.

The case parameters can be shown in Table 2. The flow diagram of numerical simulations is shown in Fig. 2. After initialization, the
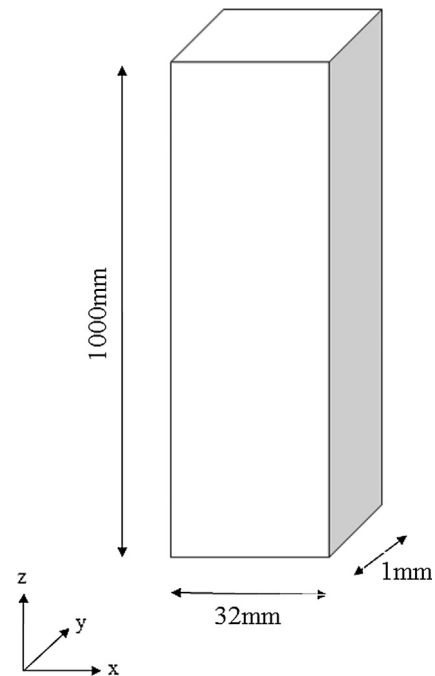

Fig. 1. Schematic diagram of the geometry of the pseudo-2D bed.

Table 1
Simulation parameters.

Parameter	Value	Unit
Gas temperature, T	293	(K)
Shear viscosity of gas, μ_g	1.8×10^{-5}	(Pas)
Molar mass of gas, M	2.9×10^{-2}	(kg/mol)
Number of particles, N_{part}	40,500	(–)
Number of particles 1, N_{part1}	20,250	(–)
Number of particles 2, N_{part2}	20,250	(–)
Diameter of particle 1, d_{a1}	1.2×10^{-1}	(mm)
Diameter of particle 2, d_{a2}	1.85×10^{-1}	(mm)
Density of particle, ρ_s	2400	(kg/m^3)
Inlet gas velocity, U_g	1.0	(m/s)
Normal restitution coefficient, e_n	0.97	(–)
Normal restitution coefficient wall, $e_{n,w}$	0.97	(–)
Tangential restitution coefficient, e_t	0.33	(–)
Tangential restitution coefficient, $e_{t,w}$	0.33	(–)
Friction coefficient, μ	0.1	(–)
Normal spring stiffness, k_n	7.0	(–)
Tangential spring stiffness, k_t	2.0	(–)
Time step, dt	2.0×10^{-5}	(s)

Table 2
Case parameters.

Case number	Without magnus	With magnus
1	$Re_r \sim 10^0$	$Re_r \sim 10^0$
2	$Re_r \sim 10^1$	$Re_r \sim 10^1$
3	$Re_r \sim 10^2$	$Re_r \sim 10^2$

new position and velocity of particles as well as local porosity are updated by use of the soft-sphere model described in Section 2.2.3. Then the governing equations in Section 2.1 will be solved, and the fluid field and particle position and velocity at this time step are calculated and saved.

3. Results

According to Ibsen et al. [34], the discrete particle simulation should run sufficiently long time to ensure the whole system reaches the steady state. In this research, we simulated 16 s physical time and the time step is 2.0×10^{-5} s. Only the results in the last 5 s were used for data analysis. The results of force, particle velocity and particle velocity fluctuation which present in this work is averaged for the last 5 s.

For analyzing the influence of Magnus effect, firstly, Magnus lift force for every standalone particle in each case is counted and compared with drag force. Secondly, particle velocity distribution in two models are calculated. Subsequently, regional particle velocities is discussed in each case. Finally, the particle velocity fluctuation curves are used to analyze different rotational Reynolds number case.

The results and analysis will meanly focus on the z-component of the particle velocity. Because in pseudo-2D system, the particle velocity in y-component can be neglected. Particle velocity on x-component will also be discussed for assistant analysis.

The Re_r plays an important role in the Magnus effect according to the definition of the Magnus lift force in Section 2.2.3 and will be set as an independent variable in this study. In this work, three Re_r values are considered: 1, 10, and 100. According to the definition of the Re_r, the value of the Re_r can be changed through modification of any of three parameters. The first option is modification of a gas parameter such as dynamic viscosity or gas velocity. The second option is modification of particle size. The third option is to change the rotation speed. If we set the first two parameters as independent variables, the drag force will be changed accordingly. Thus, in formal simulation experiments, we change the rotation speed artificially to ensure that only the Magnus lift force is different in different three case. We believe this approach can highlight the effect of the Magnus lift force instead of the combined effect of the Magnus lift force and the drag force.
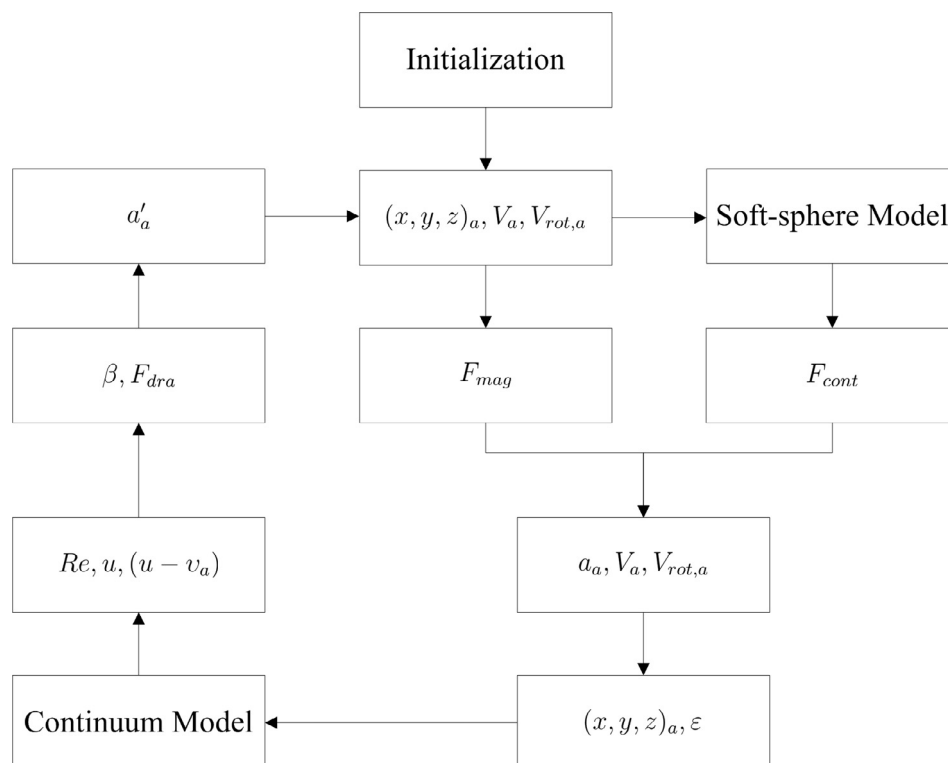

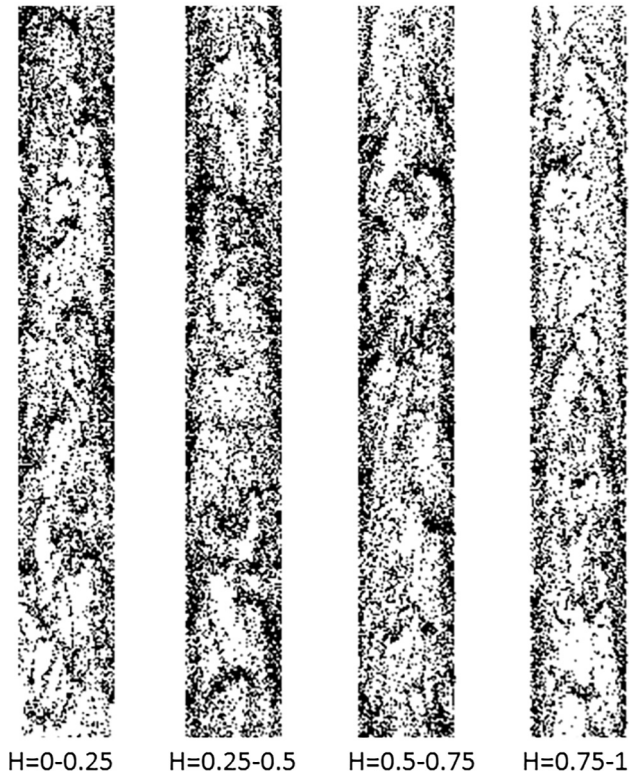**Fig. 2.** The flow diagram of numerical simulations.

Fig. 3. The snapshots of the instantaneous position of particles in the riser.

H=0-0.25   H=0.25-0.5   H=0.5-0.75   H=0.75-1

3.1. Particle positions

Instantaneous particle positions for different values of Re_r were simulated in the CFB riser. Fig. 3 shows the typical results at t = 13 s. The particles are dilute in the core region and dense in the wall region, consistent with the results of Mathiesen et al. [28]. The shape of particle cluster in some region is parabolic, which indicates the particles move upward at a faster speed near the central of the riser and downward at a slower speed near the sidewalls.

3.2. Effect of the Magnus lift force

Drag force is considered as the major force which impact particle movement in fluidized bed. Therefore, the ratio among Magnus lift force and drag force is important for analyzing the impact of Magnus lift force in fluidized bed. Fig. 4 shows the percentage of particles classified by $F_{zmag,a}/F_{zdra,a}$ in different case. As can be seen in Fig. 4(a), the $F_{zmag,a}/F_{zdra,a}$ for most particles is smaller than 0.01, which is exclusively smaller than 0.1, which means the Magnus lift force is negligible compared to the drag force when $Re_r \sim 10^0$. This can also be evidenced by Zhou and Fan [16], the lower the Reynolds number, the weaker the Magnus effect. In Fig. 4(b), the percentage of particles with $F_{zmag,a}/F_{zdra,a}$ in the range of 0.01–0.1 is higher, which suggests the Magnus lift force at $Re_r = 10$ would affect the particle motion. For even higher Re_r as showed in Fig. 4 (c), the magnitude of Magnus lift force, though less than that of drag force, becomes more pronounced. For some particles, these two forces are even in the same magnitude. Therefore, Magnus lift force might have an apparent influence on the movement of particles.

3.3. Particle velocity distribution

We analyze the particle velocity distribution for explaining the impact of Magnus lift force. The low Re_r case cannot reflect the
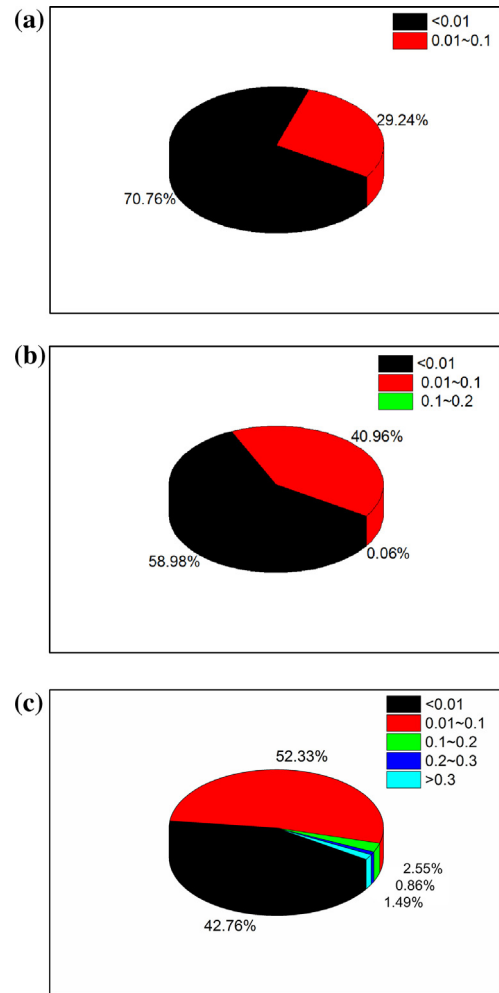

Fig. 4. The percentage of particles classified by $F_{zmag,a}/F_{zdra,a}$: (a) case 1; (b) case 2; (c) case 3.

effect of Magnus lift force according to the result in Section 3.2. Therefore, we discuss the particle velocity distribution for high Re_r case. Particle normal velocity distribution is showed in Fig. 5 (a). The particle velocities in three directions were considered separately in Fig. 5(b)–(d). At X and Y-direction, particle velocity distribution is Maxwell distribution which indicate the homogeneity of particle velocity distribution in this two directions. The gas velocity at Z-direction is much higher than other two directions. On one hand this lead to higher drag force at Z-direction. On the other hand according to Eq. (13), the influence of Magnus lift force at Z-direction will be much lower than other two directions if u_z is far larger than u_x and u_y. The difference between two curves: with or without Magnus lift force in Fig. 5(d) proved the existence of this Magnus effect at Z-direction. For high Re_r case, Magnus lift force may change the trajectory of particles.

3.4. Regional particle velocity

Regional particle velocity is another important standard to reflect the effect of Magnus lift force. According to the result in Section 3.3, even in high Re_r case the impact of Magnus lift force on particle velocity on X- direction and Y-direction can be neglected. Therefore in this section we discuss Regional particle velocity on Z-direction. Figs. 6–8 plot the radial profiles of particles vertical velocity. The results are compared with the experimental data by Mathiesen et al. [28]. There are some differences between
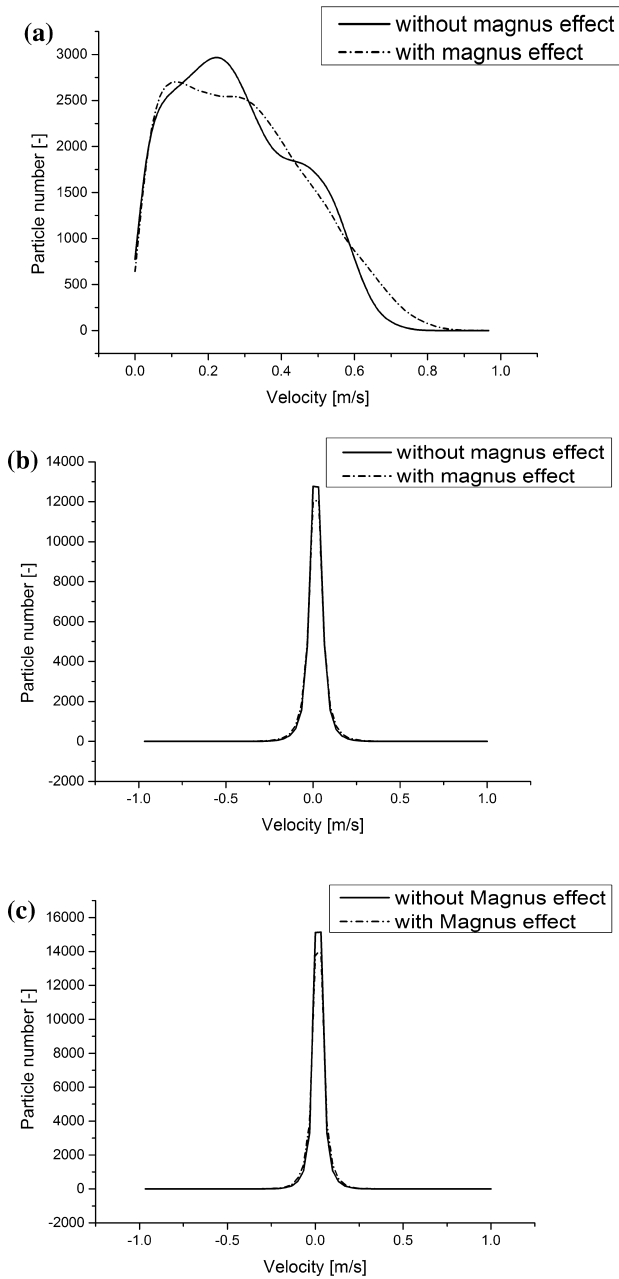
Fig. 5. Particle normal velocity distribution in case 3: (a) normal velocity distribution; (b) X-direction velocity distribution; (c) Y-direction velocity distribution; (d) Z-direction velocity distribution.
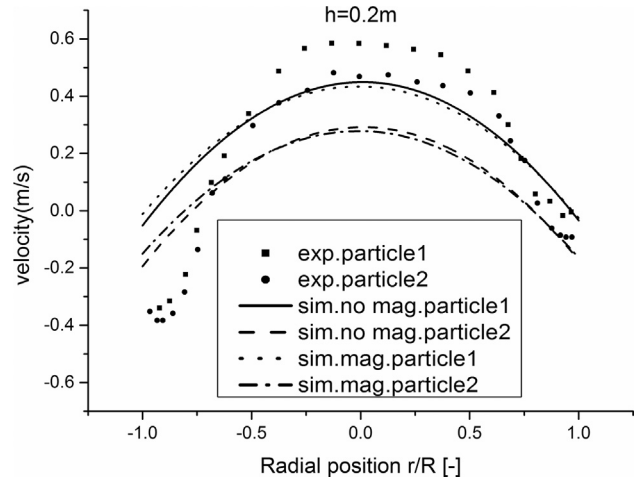

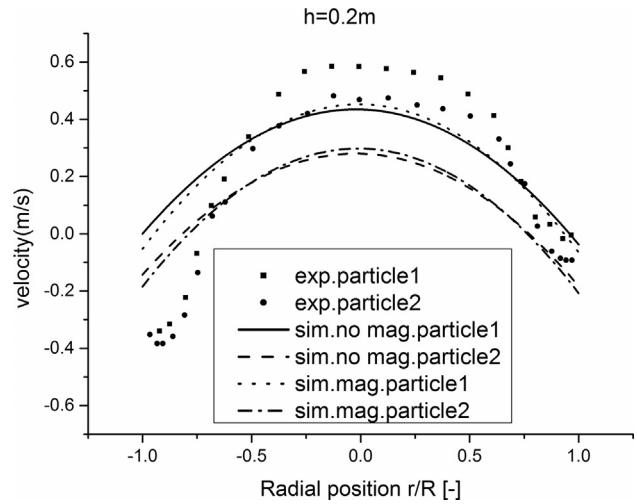**Fig. 6.** Radial profiles of Z-direction velocity at different height in case 1, h = 0.2 m.

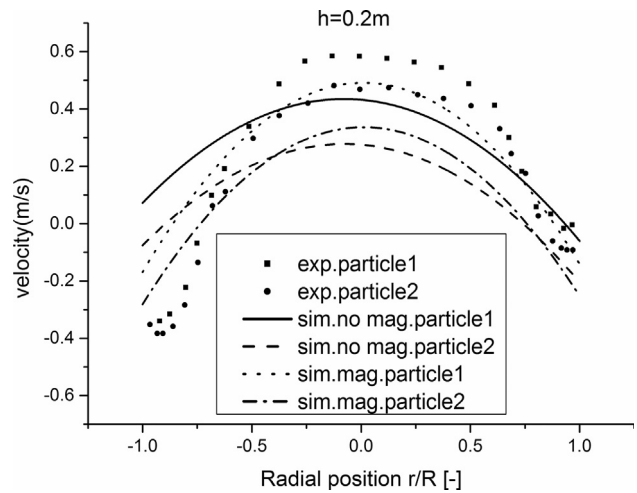**Fig. 7.** Radial profiles of Z-direction velocity at different height in case 2, h = 0.2 m.

Fig. 8. Radial profiles of Z-direction velocity at different height in case 3, h = 0.2 m.

experiment and simulation results. In the wall regions, simulation results are high than experimental results. Besides, at h = 0.2 m, the velocities are not correctly predicted very well. The velocities in core regions are lower than experiment while in wall regions are higher than experiment. The probably reasons are as follows: Firstly, particles at h = 0.2 m suffer from more fierce collision in real fluidized bed which result in the expansion of different velocities between wall regions and core regions. Secondly, this might well be related to the boundary conditions for fluid and particles which has been set in simulation model, leading to an artificial entry length in the flow. Finally, the different methods on how to deal with data might be another reason. The experiment results based on the mean values of 3000 accept simples, but simulation results are averaged for the last 5 s which make the curve become more smooth.

In case 1 and case 2 there is little difference between two models: with or without Magnus effect. Because drag force is the primary factor influencing particle movement. Fig. 8 shows the

results for Re_r = 100. In high Re_r case, little difference between the model with Magnus lift force and without Magnus lift force can be observed. So Magnus effect can be observed on particles vertical velocity.

Fig. 9 show the axial centerline profiles of particle vertical velocity. For lower rotational Reynolds number (1 and 10), the Magnus force has a minor effect. However, for higher rotational Reynolds number (1 0 0), similar to radial profile, the Magnus lift force has a pronounced effect on particle velocity, which can even influence the translational motion of particles.

In a large quantity of previous research, Empirical formula is used to revise drag model if the simulation is not in good agree-

ment with experiment and Magnus effect is neglect. However, drag force may not be the only element which can impact particle movement according to Section 3.1. Magnus lift force equally plays a pivotal role in fluidization while Re_r is high. So the introduction of Magnus effect in DEM may be another way to fix discrete element method (DEM), especially for the high rotational Reynolds number case.

Fig. 10. Radial profiles of particle velocity fluctuation at different height in case 1.

Fig. 11. Radial profiles of particle velocity fluctuation at different height in case 2.
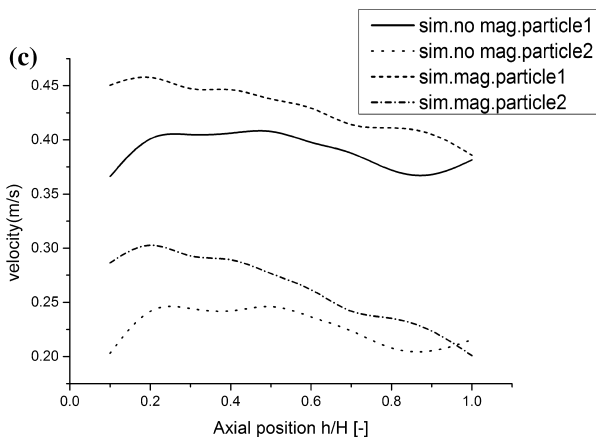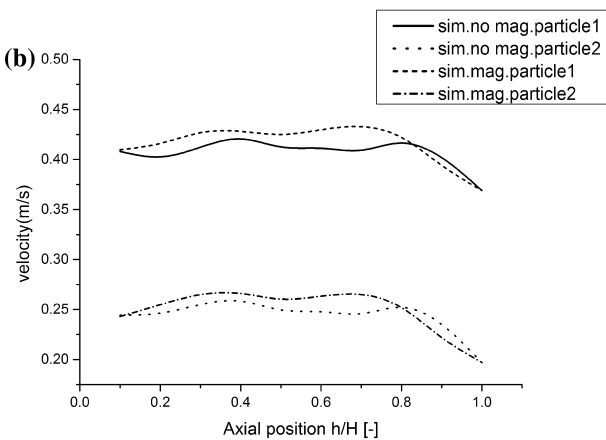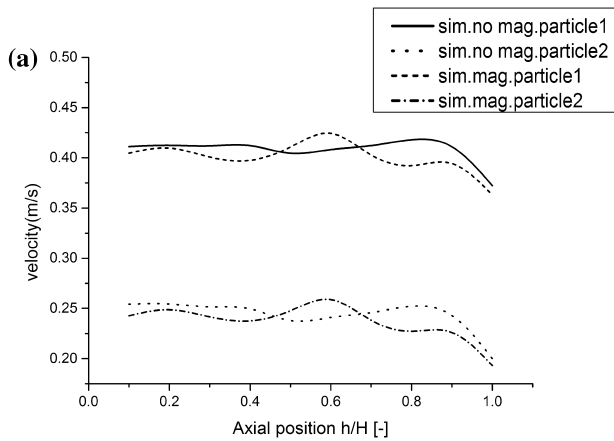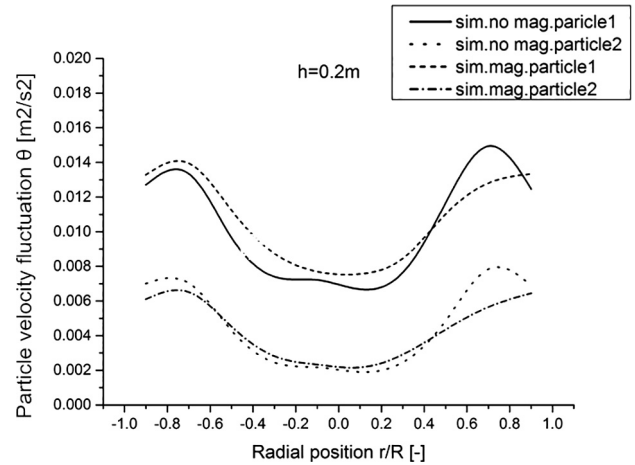

Fig. 9. Axial centerline profiles of Z-direction velocity: (a) case 1; (b) case 2; (c) case 3.

Fig. 12. Radial profiles of particle velocity fluctuation at different height in case 3.
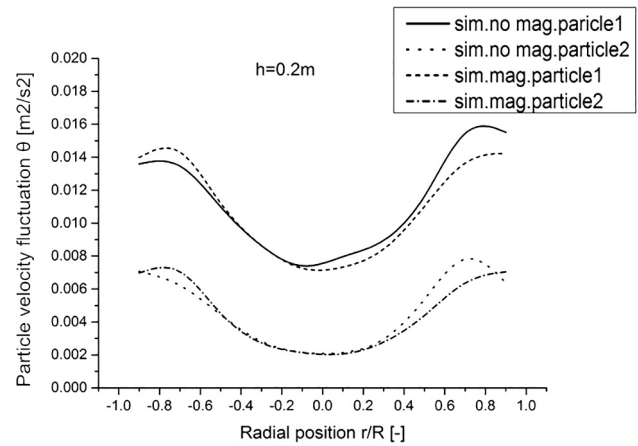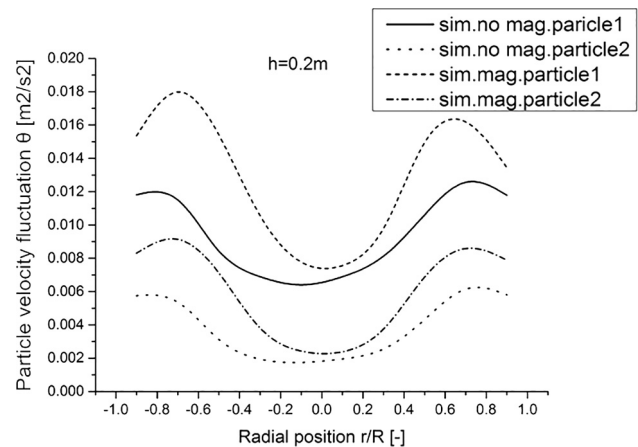
3.5. Particle velocity fluctuation

Figs. 10–12 show the particle velocity fluctuation. The fluctuation of particle velocity in Z direction is calculated:

$$\theta = \theta_z = \frac{1}{n}\sum_{k=1}^{n}(\upsilon_{z,k}^2 - \overline{\upsilon_z}^2) \tag{15}$$

Here n is the number of particles, $\overline{\upsilon}_z$ is the average velocity in Z direction:
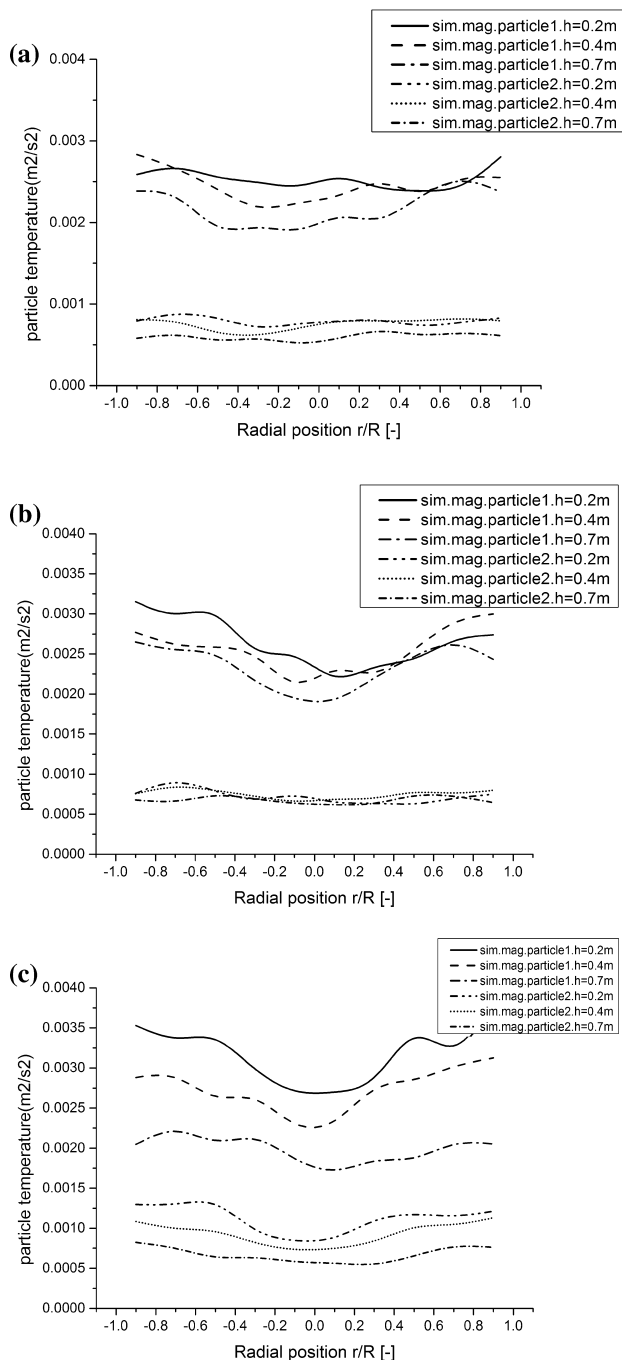
$$\overline{\upsilon_z} = \frac{1}{n}\sum_{k=1}^{n}\upsilon_{z,k} \tag{16}$$

All the curves in Figs. 10–12 show the same trend that particles fluctuate strongly near the wall and more placid in the center of riser. This may result from the effect of wall surface. According to Figs. 10 and 11 in low Re_r case, Magnus lift force is no significant effect on particles because of limited difference between two curves. Fig. 12 depicts the particle velocity for higher Re_r (~100). Compared to that for lower Re_r (1 and 10), the influence of Magnus lift force increased observably. This suggests that Magnus lift force could prompt the particle velocity fluctuation at Z-direction while Re_r is high and this mainly happened in the low part of riser.

Similar to particle velocity fluctuation at Z-direction, particle velocity fluctuation at X-direction is discussed for analyzing Radial movement. Fig. 13 show the particle velocity fluctuation at X-direction for different bed height. The influence of wall surface may be indistinctive in X-direction, and therefore the curves are smoother than that in Figs. 10–12. The particle velocity fluctuation at X-direction increases with increasing Re_r, indicating that the Magnus lift force may promote particle velocity fluctuation at X-direction only in some specific situations. The reason may be that Magnus lift force caused by particle rotation, in high Re_r case, particle rotation result in increasing instability of gas-solid system. Therefore, particle velocity fluctuation was also influenced by particle rotation. The result from this section also demonstrates that Magnus lift force may promote the radial movement of particles comparing with axial direction. Therefore, not only at Z-direction, Magnus lift force also prompts the particle velocity fluctuation at X and Y-direction.

4. Conclusions

A modified DPM code incorporated with Magnus force was used to simulation particle motion in circulating fluidized bed (CFB) risers. The results with or without Magnus lift force were compared for different Re_r numbers. The radial and axial profiles of X-direction velocity, granular temperature and radial profiles of X-direction velocity were discussed in details. Our simulations show:

1. Particles move upward with a higher speed near the central of the riser and downward with a lower speed near the walls, and the typical core-annular flow structure can be demonstrated.
2. The influence of Magnus lift force is enhanced with a higher Re_r (especially for $Re_r \sim 10^2$), and might be in the same magnitude as the drag force.
3. Magnus lift force affects the movement of particles in both radial and axial directions while Re_r is high. In low Re_r case it can be neglected in computational simulation model.

The introduction of Magnus force can improve the discrete particle model and capture the radial movement of particles in high Re_r case when used in the dilute phase region. On the other hand, in real gas-solid two phase system, high particle rotational speed might cause more prominent Magnus effect and impact particle movement. The influence of Magnus lift force still needs to be considered and evaluated in the fluidized bed when the particle rotational speed is high.

Acknowledgement

Fig. 13. Radial profiles of X-direction granular temperature: (a) case 1; (b) case 2; (c) case 3.

References

[1] Z.L. Yuan, M. Ma, Y.Q. Xu, Study on effect of particle rotation on fluidizing behavior by discrete numerical simulation method, J. Combust. Sci. Technol. 7 (2001) 238–241.

[2] L.B. Torobin, W.H. Gauvin, Fundamental aspects of solids-gas flow: Part IV: The effects of particle rotation, roughness and shape, Can. J. Chem. Eng. 38 (1960) 142–153.

[3] X. Wu, Q. Wang, Z. Luo, M. Fang, K. Cen, Theoretical and experimental investigations on particle rotation speed in CFB riser, Chem. Eng. Sci. 63 (2008) 3979–3987.

[4] X. Wu, Q. Wang, Z. Luo, M. Fang, K. Cen, Experimental study of particle rotation characteristics with high-speed digital imaging system, Powder Technol. 181 (2008) 21–30.

[5] F. Garoosi, M.R. Safaei, M. Dahari, K. Hooman, Eulerian-Lagrangian analysis of solid particle distribution in an internally heated and cooled air-filled cavity, Appl. Math. Comput. 250 (2015) 28–46.

[6] T. Kajishima, Influence of particle rotation on the interaction between particle clusters and particle-induced turbulence, Int. J. Heat Fluid Flow 25 (2004) 721–728.

[7] S. Wang, Z. Shen, H. Lu, L. Yu, W. Liu, Y. Ding, Numerical predictions of flow behavior and cluster size of particles in riser with particle rotation model and cluster-based approach, Chem. Eng. Sci. 63 (2008) 4116–4125.

[8] J. Sun, F. Battaglia, Hydrodynamic modeling of particle rotation for segregation in bubbling gas-fluidized beds, Chem. Eng. Sci. 61 (2006) 1470–1479.

[9] H.M. Barkla, L.J. Auchterlonie, The magnus or robins effect on rotating spheres, J. Fluid Mech. 47 (1971) 437–447.

[10] D.R. Oliver, Influence of particle rotation on radial migration in the poiseuille flow of suspensions, Nature 194 (1962) 1269–1271.

[11] H. Ning, Z. Xiaojing, Magnus effect in wind-blown sand saltation, J.-Lanzhou Univ. Nat. Sci. 37 (2001) 19–25.

[12] N. Lukerchenko, Collision with bed and magnus effect in numerical simulation of solid particle saltation over rough bed, in: International Conference on Computational Mechanics and Modern Applied Software Systems, Moskva, 2001.

[13] B.R. White, J.C. Schulz, Magnus effect in saltation, J. Fluid Mech. 81 (1977) 497–512.

[14] D.S. Dandy, H.A. Dwyer, A sphere in shear flow at finite Reynolds number: effect of shear on particle lift, drag, and heat transfer, J. Fluid Mech. 216 (1990) 381–410.

[15] Y. Changfu, Q. Haiying, X. Xuchang, Lift force on rotating sphere at low Reynolds numbers and high rotational speeds, Acta Mech. Sin. 19 (2003) 300–307.

[16] Q. Zhou, L.-S. Fan, Direct numerical simulation of low-Reynolds-number flow past arrays of rotating spheres, J. Fluid Mech. 765 (2015) 396–423.

[17] M. Ye, M.A.V.D. Hoef, J.A.M. Kuipers, A numerical study of fluidization behavior of Geldart A particles using a discrete particle model, Powder Technol. 139 (2004) 129–139.

[18] M. Ye, M.A.V.D. Hoef, J.A.M. Kuipers, The effects of particle and gas properties on the fluidization of Geldart A particles, Chem. Eng. Sci. 60 (2005) 4567–4580.

[19] M. Ye, M.A.V.D. Hoef, J.A.M. Kuipers, From discrete particle model to a continuous model of geldart A particles, Chem. Eng. Res. Des. 83 (2005) 833–843.

[20] J.A.M. Kuipers, K.J.V. Duin, F.P.H.V. Beckum, W.P.M.V. Swaaij, A numerical model of gas-fluidized beds, Chem. Eng. Sci. 47 (1992) 1913–1924.

[21] G.A. Bokkers, M.V.S. Annaland, J.A.M. Kuipers, Mixing and segregation in a bidisperse gas–solid fluidised bed: a numerical and experimental study, Powder Technol. 140 (2004) 176–186.

[22] J.H. Ferziger, M. Perić, Computational methods for fluid dynamics, Phys. Today 50 (1996) 80–84.

[23] P.A. Cundall, O.D. Strack, A discrete numerical model for granular assemblies, geotechnique 29 (1979) 47–65.

[24] M. Ye, Multi-Level Modeling of Dense Gas-Solid Two-Phase Flows, University of Twente, Netherlands, 2005.

[25] S. Ergun, A.A. Orning, Fluid flow through randomly packed columns and fluidized beds, Ind. Eng. Chem. 41 (1949) 1179–1184.

[26] C.Y. Wen, Y.H. Yu, Mechanics of fluidization, Chem. Engng. Prog. Symp. Ser. 62 (1966) 100–111.

[27] C.W. Oseen, Über die stoke'sche formel und über eine verwandte aufgabe in der hydrodynamik, Almqvist & Wiksell, 1911.

[28] V. Mathiesen, T. Solberg, B.H. Hjertager, An experimental and computational study of multiphase flow behavior in a circulating fluidized bed, Int. J. Multiph. Flow 26 (2000) 387–419.

[29] Y. Tsuji, T. Kawaguchi, T. Tanaka, Discrete particle simulation of two-dimensional fluidized bed, Powder Technol. 77 (1993) 79–87.

[30] D. Hu, G. Han, M. Lungu, Z. Huang, Z. Liao, J. Wang, Y. Yang, Experimental investigation of bubble and particle motion behaviors in a gas-solid fluidized bed with side wall liquid spray, Adv. Powder Technol. 28 (9) (2017) 2306–2316.

[31] C.D. Dritselis, On the enhancement of particle deposition in turbulent channel airflow by a ribbed wall, Adv. Powder Technol. 28 (3) (2017) 922–931.

[32] K.E. Cheikh, C. Djelal, Y. Vanhove, P. Pizette, S. Rémond, Experimental and numerical study of granular medium-rough wall interface friction, Adv. Powder Technol. 29 (1) (2018) 130–141.

[33] M.R. Safaei, O. Mahian, F. Garoosi, K. Hooman, A. Karimipour, S.N. Kazi, S. Gharehkhani, Investigation of micro- and nanosized particle erosion in a 90° pipe bend using a two-phase discrete phase model, Sci. World J. (2014-10-14) 2014 (2014) 740578.

[34] C.H. Ibsen, E. Helland, B.H. Hjertager, T. Solberg, L. Tadrist, R. Occelli, Comparison of multifluid and discrete particle modelling in numerical predictions of gas particle flow in circulating fluidised beds, Powder Technol. 149 (2004) 29–41.